

Eye-for-an-eye: Appearance Transfer with Semantic Correspondence in Diffusion Models

Sooyeon Go Kyungmook Choi Minjung Shin Youngjung Uh*

Yonsei University, Seoul, South Korea

{sooyeon8658, kyungmook.choi, smj139052, yj.uh}@yonsei.ac.kr

Abstract

As pretrained text-to-image diffusion models have become a useful tool for image synthesis, people want to specify the results in various ways. In this paper, we introduce a method to produce results with the same structure of a target image but painted with colors from a reference image, i.e., appearance transfer, especially following the semantic correspondence between the result and the reference. E.g., the result wing takes color from the reference wing, not the reference head. Existing methods rely on the query-key similarity within self-attention layer, usually producing defective results. To this end, we propose to find semantic correspondences and explicitly rearrange the features according to the semantic correspondences. Extensive experiments show the superiority of our method in various aspects: preserving the structure of the target and reflecting the color from the reference according to the semantic correspondences, even when the two images are not aligned. You can visit https://sooyeon-go.github.io/eye_for_an_eye/.

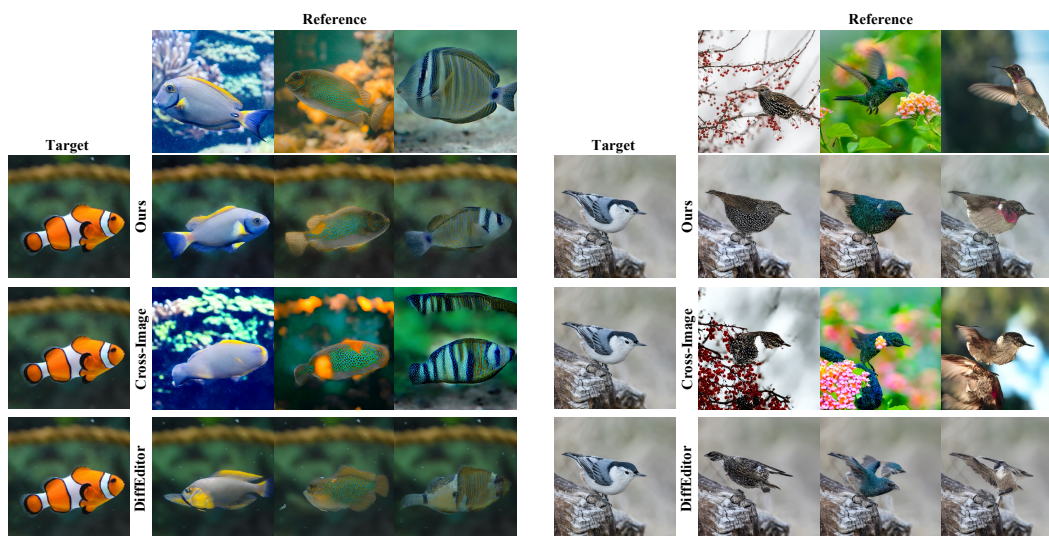


Figure 1: Our method transfers semantically corresponding appearances from reference images to target images. In contrast to other methods such as DiffEditor [23] and Cross-Image [1], our method preserves the structure of the target images successfully transfers the colors and patterns considering the semantic meanings from the references.

*Corresponding author

1 Introduction

Text-to-image diffusion models [28] generate high quality realistic images, allowing users to specify the desired results using simple textual inputs. Furthermore, some variants receive images whose elements will appear in the results. Editing methods [3, 32, 7] make partial changes in a scene while keeping the rest unchanged. ControlNet variants [36] produce images with shapes specified by input skeletons or depth maps.

We tackle a scenario with two input images where the result has the shape of one image and the color pattern of another, often called appearance transfer from a reference image to a target image. Previous methods [1, 23, 22, 9] primarily addressed cases with self-attention injection and feature guidance. In these cases, each object in the target image and the reference image are mostly well-aligned when we define 'well-aligned' as cases where the pose or direction of the target object and the reference object same. However, finding a reference sample properly aligned with the target object is challenging. Therefore, it is crucial to address appearance transfer in cases where the objects are unaligned. Existing methods have the following limitations as shown in Figure 1. 1) They transfer appearance from an object to misaligned regions of a target, e.g., fin to mouth. This leads to a discrepancy in a sequence of color arrangement between the output and the reference object. For example, The reference wing color is transferred to the head region of the target. It happens due to a lack of semantic matches between the self-attention key of reference and the query of the target. 2) The detailed pattern of the reference object may disappear or be distorted when it is transferred to the output image. It occurs due to a noise guidance, which equalizes the average features of different objects.

To this end, we propose to execute semantic matching-based appearance transfer in a training-free manner. Semantic matching-based appearance transfer is a method that paints the appearance (e.g., color, pattern) of the reference image based on the target image, considering positions aligned with semantic correspondence. Our method tackles two sub-problems: finding semantic correspondences and transferring appearances. We find a correspondence in features to enable obtaining more semantically meaningful matching than self-attention. However, even with the method of finding correspondence in features, there are samples where object features match with the background. To prevent these cases, we utilize image-level segmentation to perform semantic matching among objects. Based on our semantic alignment, we rearrange the reference features according to the correspondence and inject them to replace the target features. Instead of existing methods, which preserve the queries of a target image and inject only keys and values from a reference image, ours brings the rearranged query, key, and value. Through our approach, we mitigate incorrect transfer problems from a semantic mismatch between queries and keys across different images.

Ours enables accurate appearance transfer to the precise locations. We achieved this even in samples with complex colors and patterns or different views and poses. Additionally, by transferring the appearance information to the target structure, our method excels in preserving the target's structure both qualitatively and quantitatively. We also analyze the optimal components in the diffusion process for semantic-based appearance transfer. Furthermore, our method can be extended to perform appearance transfer across different domains and to transfer different appearances to multiple objects.

2 Related Work

Attention features for image editing Recent approaches [13, 11, 25, 19, 31, 4, 1, 20, 26, 8] manipulate the attention layers of pretrained diffusion model for image editing. Image-to-image translation methods leverage attention maps from the cross-attention layer as attention re-weighting [13], swapping [11] and cross-attention guidance [25, 19]. MasaCtrl [4] and Cross-Image [1] replace the key and value features in the self-attention layer, known as key-value injection, to achieve text-guided translation of reference images. In addition to key-value injection, PnP-diffusion [31] manipulates spatial features that contain fine-grained spatial information. Because the self-attention layers contain semantic information, modifying attention features can be used for downstream editing tasks without the need for fine-tuning.

Appearance transfer Appearance transfer produces an image that combines the shape and color patterns of two different images. This is accomplished by training on each target domain [10, 5, 24] and using either input image pairs [30] or using external models to guide diffusion model [17]. These approaches effectively preserve the target image's structure but perform poorly with unaligned images

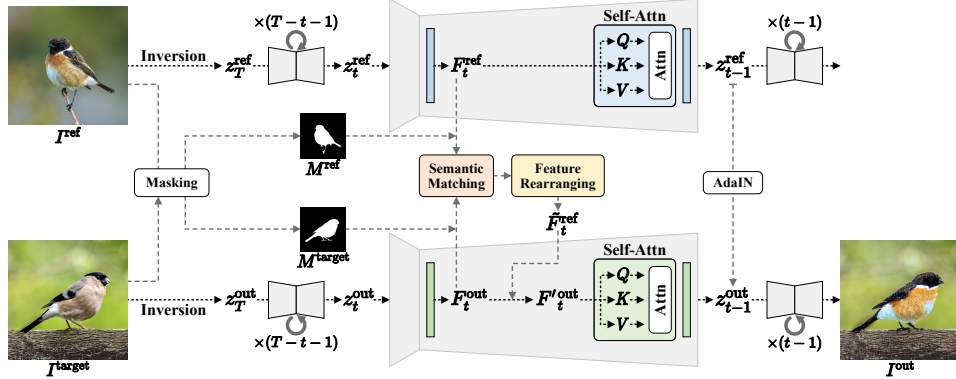


Figure 2: **Pipeline of our method.** We transfer the semantically corresponding appearance of objects from a reference image to a target image. Given I^{ref} , I^{target} , and their masks M^{ref} and M^{target} , we find semantic correspondences between their self-attention features F_t^{ref} and F_t^{out} . Then, we inject the rearranged features based on these correspondences.

or those from different domains. Recent approaches [9, 22, 23, 1] excel with images from different domains without requiring fine-tuning. However, self-guidance [9] leads to discrepancies in color distribution between the output and reference image due to noise guidance, which makes the average feature values of the output and reference image similar. Cross-Image [1] uses query-key attention scores with key-value injection from the reference image to semantically similar pixels in the target image. Dragon-diffusion [22] and DiffEditor [23] incorporate both noise guidance and key-value injection. Despite this, these methods struggle to preserve structure and often fail with unaligned samples. As illustrated in Figure 3, attention scores derived from queries and keys from different images often fail to achieve semantic alignment for unaligned or complex samples. In contrast, we transfer appearance by explicitly rearranging features based on their semantic correspondence.

Semantic correspondence Leveraging the diffusion features of a model trained on large image-text pairs, unsupervised semantic correspondence methods [12, 29] outperform other weakly-supervised methods. SD-DINO [35] further enhances performance by combining DINO ViT [2] as an additional feature extractor. Recent approaches [31, 34, 4] demonstrate that the inherent semantic understanding of diffusion models is distributed across diffusion timesteps and U-Net layers. Consequently, diffusion Hyperfeatures [21], which aggregates features extracted across multiple diffusion timesteps and U-Net layers, achieve a significant improvement in correspondence matching accuracy. To ensure that image editing aligns with the semantics of each step and layer, we separately rearrange the feature maps based on their corresponding semantic matches in each timestep and U-Net layer.

3 Method

We aim to transfer local appearances from a reference image I^{ref} to a target image I^{target} according to semantic correspondences between them. As shown in Figure 2, our method produces an image from a denoising process starting from an inversion [15] of I^{target} (bottom) with modifications from another denoising process starting from an inversion of I^{ref} (top). The modification includes finding semantic correspondences between the two denoising processes and injecting features with rearrangement.

3.1 Motivation

Recent methods [4, 1, 22] with frozen Stable Diffusion [28] adopts key-value (KV) injection in self-attention layers: replacing key, and value in a target denoising process with the ones from a reference denoising process. Self-attention for a given feature map $F \in \mathcal{R}^{hw \times c}$ is defined by $\text{softmax}(QK^T/\sqrt{d_k})V$ where $Q = FW^{\text{query}}$, $K = FW^{\text{key}}$, $V = FW^{\text{value}}$, $W^{\text{query,key}} \in \mathcal{R}^{c \times d_k}$, and $W^{\text{value}} \in \mathcal{R}^{c \times d_v}$. $(QK^T/\sqrt{d_k})$ computes the similarity between a query and the keys and its row corresponding to a pixel $\mathbf{q} \in [0, h) \times [0, w)$ is called an attention map. Figure 3 (a,e) shows examples of self-attention maps for two pixels in the targets. Multiplying an attention map to V

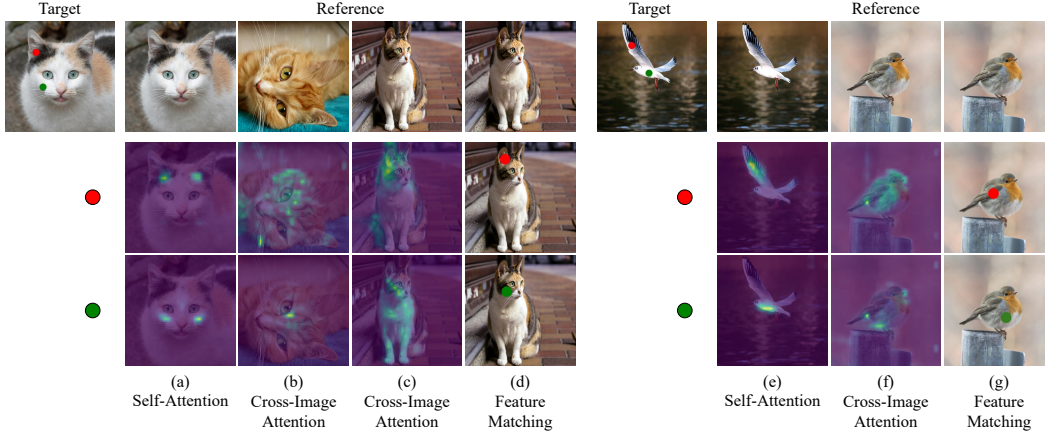


Figure 3: **Query-key attention maps vs. our feature matching.** For each query pixel \mathbf{q} denoted as colored markers in the target image, we show the attention maps based on the QK attention score.

produces aggregation of V weighted by the attention map which will be assigned to the location of the query. Hence, the self-attention with KV injection from a reference denoising process computes aggregation of the reference V weighted by the similarity between each target query and the reference keys and assigns the aggregation to each pixel in the target. As a result, the generated image has the rearranged visual elements from the reference according to the semantic spatial arrangements of the target.

Although the KV injected attention map is the similarity between a pixel in the target feature map F^{out} and all pixels in the reference feature map F^{ref} , the similarity does not necessarily reflect the semantic correspondence between the target image and the reference image. For example, in Figure 3 (c), the attention map for the cheek (green dot) does not highlight the cheek in the reference but in other parts. It especially malfunctions when the target and reference images are not aligned. In such cases, the previous methods with KV injection produce unexpected results as shown in Figure 1.

3.2 Semantic matching-based feature rearranging

As described in Sec. 3.1, previous appearance transfer methods with KV injection do not always reflect *semantic* correspondences between the reference and the target. On the other hand, we explicitly rearrange the reference feature map to match the spatial arrangement of semantics in the target during the target denoising process.

To find the semantic correspondence of a query pixel \mathbf{q} among the reference pixel \mathbf{p} , we take $\arg \max$ of the cosine similarity in the feature map before l -th self-attention layer at denoising timestep t :

$$\mathbf{p} = \arg \max_{\mathbf{p} \in [0, h) \times [0, w)} \text{sim}(F^{\text{out}}(\mathbf{q}), F^{\text{ref}}(\mathbf{p})), \quad (1)$$

where $F^{\text{out}} \in R^{hw \times c}$ is the target feature map, $F^{\text{ref}} \in R^{hw \times c}$ is the reference feature map, and sim computes cosine similarity. l and t are omitted from $F_{l,t}^*$ for brevity.

Then, we rearrange the reference feature map to be $\tilde{F}^{\text{ref}}(\mathbf{q}) = F^{\text{ref}}(\mathbf{p})$.

Our matching is inspired by DIFT [29] which computes the similarity between two images in the diffusion features. While DIFT computes the similarity between inversions, i.e., *fixed* denoising processes, our method computes the similarity between a fixed inversion of the reference and the *modified* denoising process of the target.

Diffusion features at different layers l and timesteps t encode different aspects of an image [4, 34, 18]. To achieve appearance transfer with semantic correspondences, we rearrange features with semantic correspondences found at each t and l separately in multiple timesteps and layers: $t \in [42, 100]$ and layer $l \in [2, 3]$ from the up-blocks of U-net. On the other hand, DIFT computes correspondences from a single timestep and a single layer. The results from our method are more realistic and have fewer artifacts than the ones from fixed matching, i.e., DIFT. We defer the comparison between

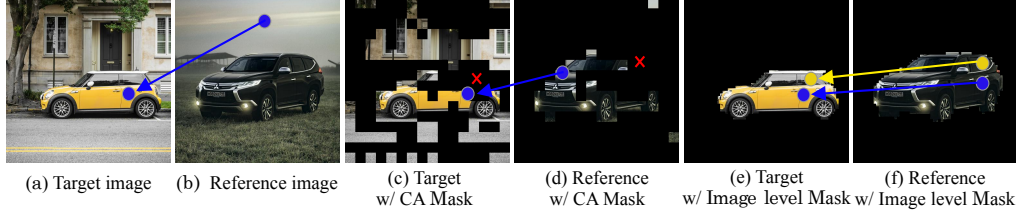


Figure 4: The blue points in (a) and (b) illustrate the case where the target object matches the reference background. In (c) and (d), the cross-attention mask prevents matching with the background. However, the mask does not effectively separate the object from the background. In (e) and (f), using image-level masks accurately separates the object from the background, enabling successful semantic matching.

ours (i.e., semantic matching found at each timestep is used for each rearrangement) and DIFT (i.e., semantic matching found at one timestep is consistently used for rearrangement in all timesteps) to §4.4.

3.3 Matching within masks

While our matching method is superior to attention and DIFT, it occasionally produces wrong matches. Figure 9 (d) shows an example where our correspondence connects mismatching regions, e.g., a car and a pavement. To this end, we confine the correspondence within the region of interest by employing masks. As shown in Figure 4 (c) and (d), a cross-attention mask utilized in prior works[4] produces low-resolution masks often being inaccurate.

In contrast, we obtain masks of the pixel resolution by feeding the images to an off-the-shelf segmentation model as shown in Figure 4 (e) and (f). Given the reference image mask M^{ref} and target image mask M^{target} , we obtain the masked features as follows:

$$F_{\text{masked}}^{\text{out}}, F_{\text{masked}}^{\text{ref}} = F^{\text{out}}[M^{\text{target}}], F^{\text{ref}}[M^{\text{ref}}]. \quad (2)$$

Then, replacing F^{out} and F^{ref} in Eq. 1 with $F_{\text{masked}}^{\text{out}}$ and $F_{\text{masked}}^{\text{ref}}$ achieves accurate correspondences.

3.4 Rearranged feature injection

Finally, we inject the rearranged reference features into the target features on the target mask:

$$F'^{\text{out}} = \tilde{F}_m^{\text{ref}} \odot M^{\text{target}} + F^{\text{out}} \odot (1 - M^{\text{target}}), \quad (3)$$

where \odot represents the Element-wise product. Then the self-attention becomes

$$\text{softmax} \left(\frac{Q'^{\text{out}}(K'^{\text{out}})^T}{\sqrt{d}} \right) V'^{\text{out}}, \quad (4)$$

where $Q'^{\text{out}} = F'^{\text{out}}W^{\text{query}}$, $K'^{\text{out}} = F'^{\text{out}}W^{\text{key}}$, and $V'^{\text{out}} = F'^{\text{out}}W^{\text{value}}$.

Additionally, the transferred output often has different color brightness and contrast when compared to the reference. To address this issue, we apply AdaIN[14] used in Cross-Image [1] to masked noise, thereby reducing the appearance color discrepancy between the reference and the output.

4 Experiments

Competitors We compare our results with recent training-free diffusion-based methods, including Cross-Image [1], which uses KV injection, DiffEditor [23], which shows the best result among methods with score-based editing guidance [9, 22, 23], and DiffuseIT [17], which leverages external models for guidance. In addition, we compare our method with the optimization-based approach Splice ViT [30] and the domain-specific trained Swapping Auto-Encoder (Swapping AE) [24]. All experiments were conducted at a resolution of 512^2 , except for the Swapping AE and DiffuseIT, which were trained at a resolution of 256^2 . In Appendix C, we provide more details on implementation and hyperparameters for each method.

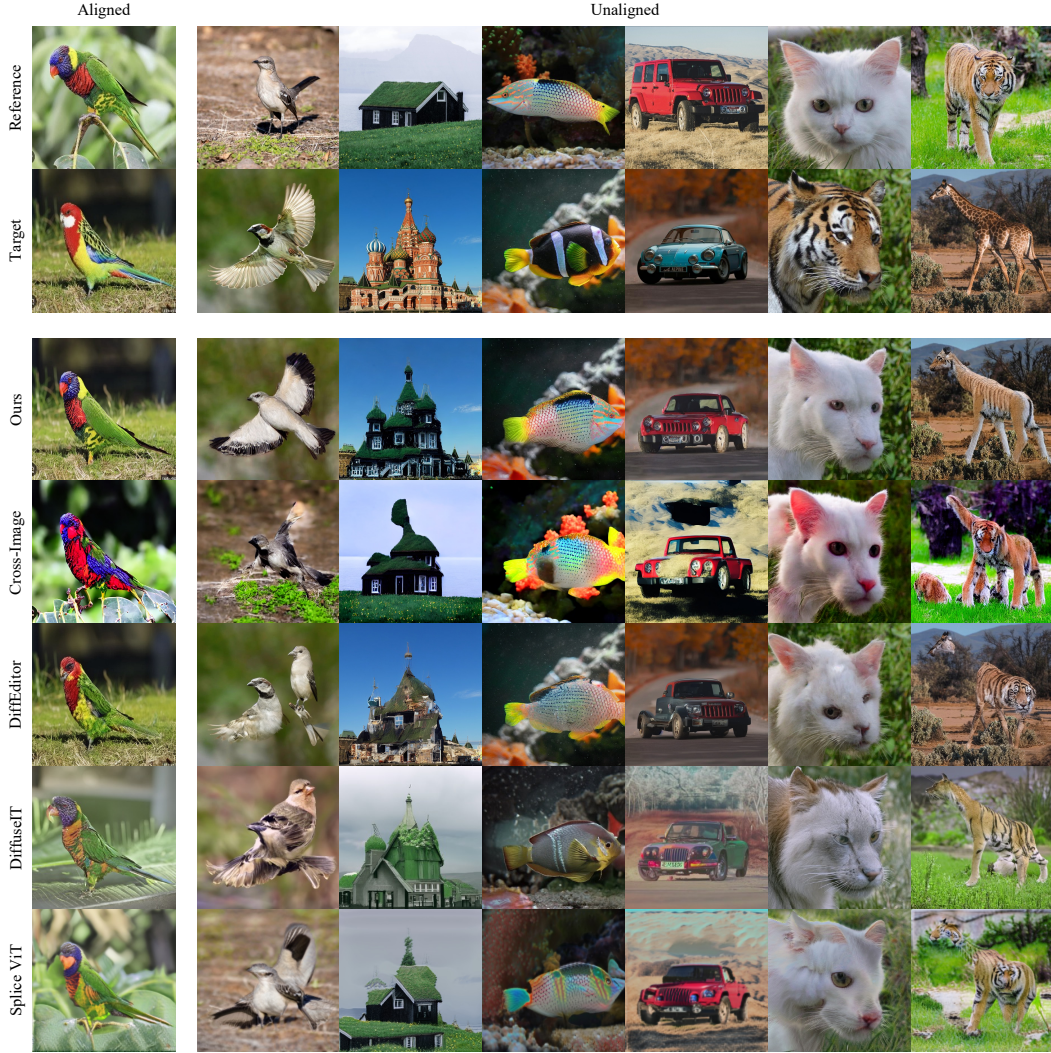


Figure 5: **Qualitative comparison** for the cases where the target and reference objects are aligned and unaligned. "Aligned" refers to objects with similar poses and sizes. "Unaligned" refers to the rest. The red box indicates instances where the structure of the target is not preserved. The blue box represents cases where the background's appearance blends into the object. More comparison samples are provided in Appendix F.

4.1 Appearance transfer with correspondence matching

Complex patterns The first column in Figure 5 demonstrates that our method transfer complex color arrangements according to the semantic correspondence, e.g., the result has a blue head, green wings, and a red-plus-green body just as the reference does. On the other hand, the competitors fail in various ways. Note that this example is an easy case where the target and the reference are aligned.

Robustness to unaligned pairs Even when the target and reference are not aligned, our method successfully transfers the correct appearance from the references to the targets while the competitors mostly fail. The right block in Figure 5 shows examples where our method achieves wing-to-wing, roof-to-roof, and fin-to-fin transfer, etc. Detailed analysis is deferred to 4.3.

In addition, the appearance outside the region of interest does not intrude in our method, while others struggle. Blue boxes in Figure 5 highlight intrusion of background appearances.

Figure 6 compares our method with Swapping AE on its domains. Yellow boxes in Figure 6 show that Swapping AE often fails to reflect the references even with exhaustive hyperparameter tuning. In

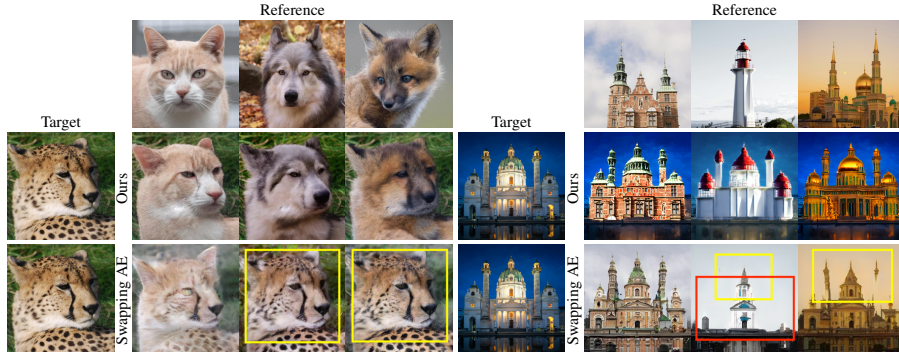


Figure 6: **Comparison with Swapping AE [24]** pretrained on AFHQ and LSUN church [33]. The yellow box indicates a failure case where the appearance of the reference image does not emerge.

	Structure Preservation (IOU \uparrow)					
	Ours	Cross-Image	DiffEditor	DiffuseIT	Splice ViT	Swapping AE
Building	0.939	0.758	0.863	0.855	0.842	0.821
AFHQ	0.972	0.915	0.943	0.951	0.943	0.942

Table 1: **Quantitative evaluation for structure preservation.** We compute the IoU between object masks derived from the original target image and the output image. We mark the highest score in red and the second-highest score in yellow.

contrast, our method successfully transfers colors and patterns to the corresponding regions, such as the distinct areas of animal faces or the roofs and walls of buildings.

4.2 Structure preservation

Qualitative evaluation As shown in the unaligned examples in Figure 5, only our method preserves the structure of the target object in the transferred results. It is possible due to the design of our method with semantically corresponding rearrangement and masked injection on the up-block of U-Net. The building examples in Figure 6 show that our method preserves all five towers while Swapping AE loses some towers.

Quantitative evaluation We evaluate the performance of structure preservation using the intersection over union (IoU) between the results and the target image. We employ an off-the-shelf model [16] to obtain object masks and perform evaluations only within the object regions. Table 1 compares IoU on two datasets: Buildings and AFHQ [6]. The buildings are collected from Pexels² and web search. This dataset will be publicly available. Our method achieves the highest IoU in both domains. Please check the detail of evaluation protocol in Appendix B.

4.3 Analysis of rearrange and injection component

Figure 7 illustrates (a) an example where humans expect the appearance of the reference belly to transfer to the target belly, (b) a belly with a mixture of different colors, (c) the behavior of our feature map injection, $\text{on } F$, compared to key-value injection and value injection, $\text{on } KV$ and $\text{on } V$, respectively.

Briefly, $\text{on } KV$ and $\text{on } V$ produce red smudges in the belly while $\text{on } F$ produces a clear lime-like belly, correctly reflecting the reference. Each row in Figure 7(c) visualizes attention maps for the red dot in the target over the denoising timesteps. $\text{on } F$ aggregates visual elements from the lime-colored reference belly following the semantics. On the other hand, $\text{on } KV$ and $\text{on } V$ attend red neck and red head, ignoring the semantics.

We suggest the reason as follows. In self-attention, Q determines the output for given the same K and V , i.e., pixels with the same feature vector in Q will have the same output through the attention mechanism, because their attention maps will be the same. Our method rearranges the reference F according to the semantic correspondence to the target and replaces the target F with it. Hence, our

²<https://www.pexels.com/>

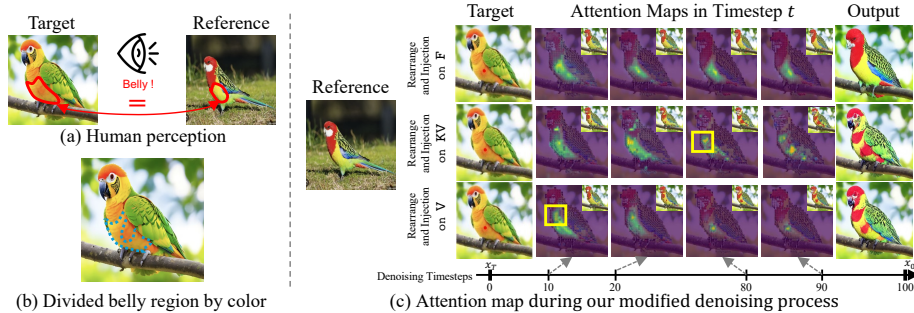


Figure 7: **Comparison of attention maps.** (a) shows the corresponding region between the target and the reference from human perception. (b) illustrates dividing regions based on color, not semantic meaning. (c) provides the attention maps for the target image’s query pixel (red dot) at different timesteps during appearance transfer. The K&V modification (first row) and V modification (second row) perform semantic matching in the same manner as our method but apply the rearrangement and injection processes to K&V and V instead of the feature map, respectively. The image at the top right of each attention map represents the result of feature rearrangement, which is indirectly shown by rearranging the reference RGB image with semantic matching calculated from U-Net’s 2nd up-block.

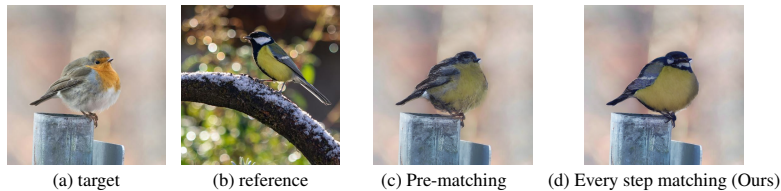


Figure 8: Pre-matching (c) calculates semantic matching between feature maps on a specific denoising step and applies the pre-matching results to other steps. Our method (d) computes the semantic matching at every step and applies them to the feature arrangement processed at each step.

results have the visual elements of the reference arranged in the semantic structure of the target. In contrast, on KV and on V keep the target Q which leads to high attention from the orange-ish belly in the target to red parts in the reference as shown in the attention maps (yellow boxes in Figure 7 (c)).

4.4 Analysis of semantic matching step

We demonstrate that our semantic matching method, which considers the similarity between features at each denoising step, is suitable for appearance transfer. Our approach for comparing similarity between features for semantic matching is inspired by DIFT [29]. DIFT matches semantic information using feature maps at a fixed denoising step. We compare the results of applying DIFT’s precomputed matching to all steps for feature arrangement (Figure 8(c)) with our method, which computes matching and feature arrangement at every step (Figure 8(d)). The feature arrangement based on DIFT’s pre-matching results leads to the loss of small region colors, fine details, and patterns, such as bird wings. This result indicates that while DIFT’s semantic matching criteria are useful for finding image correspondence, they are insufficient for our task, which requires consideration of fine detail transfer. Since different attributes are processed at each denoising step [34], our semantic matching method injects features from various denoising steps to consider attributes from coarse to fine. (Appendix D)

4.5 Ablation study

In this section, we perform ablation experiments regarding different components of our method and show its contribution in Figure 9. Compared to KV injection (c), our semantic matching-based feature rearranging (d) transfers appearance to regions where the semantic meaning of objects aligns. For instance, the belly(the red arrow) and head(the yellow arrow) colors of the reference bird are transferred to the belly and head of the target bird, respectively. As shown in (e), the mask ensures better preservation of the object’s structure (*i.e.*, tail) and maintains the background of the target

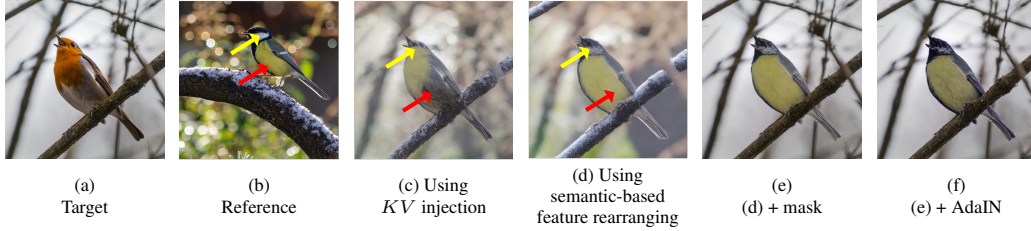


Figure 9: We perform an ablation study to validate our method.



Figure 10: Results of various applications

image. In (f), the AdaIN on masked noise matches the global color distribution of the object, thereby maintaining the color brightness and contrast of the appearance object. We provide more samples of ablation in Appendix E.

4.6 Application

Cross-category/style appearance transfer Our method enables semantic matching-based transfer even in challenging samples where the target object and the reference object belong to different categories or exhibit different styles. In Figure 10, (a) shows a bird’s appearance plausibly transferred to an airplane, while (b) depicts the appearance of a real rabbit applied to a Disney-style rabbit.

Multi-objects appearance transfer Our method can individually transfer the appearance of multiple objects in the target image, each from a different reference image. Objects in the target image are matched and rearranged one by one with the reference images. Each process is executed simultaneously within a single generation process, rather than sequentially. In Figure 10, (c) presents the results with three birds in the target image, each with distinct appearances from three different images.

5 Conclusion

In this paper, we have introduced a training-free appearance transfer method using a pretrained text-to-image diffusion model. Our method faithfully reflects the reference image to the target image according to semantic correspondences, e.g., fin-to-fin and wing-to-wing, while previous methods often ignore semantics. Our key arguments for replacing features in the target denoising process with the reference denoising process are 1) reflecting semantic correspondences 2) found during the modified denoising process 3) on the input features of self-attention 4) confined in the region of interest. Experiments demonstrate that our method achieves faithful appearance transfer between the semantically corresponding parts of the result and the reference and better preserves the structure of the target in the result compared to existing methods.

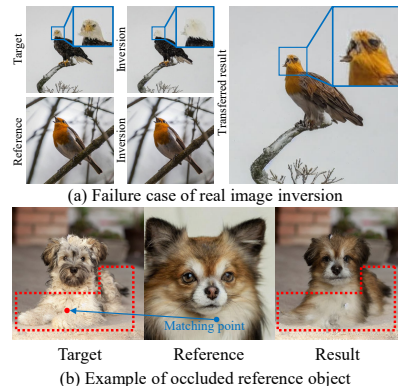


Figure 11: Results with limitations

Limitation In order to use a real image as a reference, our method relies on inversion. If the inversion malfunctions, our method struggles as shown in Figure 11 (a). Also, Figure 11 (b) shows that the reference image does not have the semantically corresponding parts from the target image

and our matching finds the most similar parts instead of semantic correspondence. Still, the results tend to be realistic in such cases.

References

- [1] Yuval Alaluf, Daniel Garibi, Or Patashnik, Hadar Averbuch-Elor, and Daniel Cohen-Or. Cross-image attention for zero-shot appearance transfer. *arXiv preprint arXiv:2311.03335*, 2023.
- [2] Shir Amir, Yossi Gandelsman, Shai Bagon, and Tali Dekel. Deep vit features as dense visual descriptors. *arXiv preprint arXiv:2112.05814*, 2(3):4, 2021.
- [3] Omri Avrahami, Dani Lischinski, and Ohad Fried. Blended diffusion for text-driven editing of natural images. In *Proceedings of the IEEE/CVF Conference on Computer Vision and Pattern Recognition*, pages 18208–18218, 2022.
- [4] Mingdeng Cao, Xintao Wang, Zhongang Qi, Ying Shan, Xiaohu Qie, and Yinqiang Zheng. Masactrl: Tuning-free mutual self-attention control for consistent image synthesis and editing. In *Proceedings of the IEEE/CVF International Conference on Computer Vision*, pages 22560–22570, 2023.
- [5] Xi Chen, Lianghua Huang, Yu Liu, Yujun Shen, Deli Zhao, and Hengshuang Zhao. Anydoor: Zero-shot object-level image customization. *arXiv preprint arXiv:2307.09481*, 2023.
- [6] Yunjey Choi, Youngjung Uh, Jaejun Yoo, and Jung-Woo Ha. Stargan v2: Diverse image synthesis for multiple domains. In *Proceedings of the IEEE/CVF conference on computer vision and pattern recognition*, pages 8188–8197, 2020.
- [7] Guillaume Couairon, Jakob Verbeek, Holger Schwenk, and Matthieu Cord. Diffedit: Diffusion-based semantic image editing with mask guidance. *arXiv preprint arXiv:2210.11427*, 2022.
- [8] Yilun Du, Joshua Meier, Jerry Ma, Rob Fergus, and Alexander Rives. Energy-based models for atomic-resolution protein conformations. *arXiv preprint arXiv:2004.13167*, 2020.
- [9] Dave Epstein, Allan Jabri, Ben Poole, Alexei Efros, and Aleksander Holynski. Diffusion self-guidance for controllable image generation. *Advances in Neural Information Processing Systems*, 36:16222–16239, 2023.
- [10] Vidit Goel, Elia Peruzzo, Yifan Jiang, Dejjia Xu, Nicu Sebe, Trevor Darrell, Zhangyang Wang, and Humphrey Shi. Pair-diffusion: Object-level image editing with structure-and-appearance paired diffusion models. *arXiv preprint arXiv:2303.17546*, 2023.
- [11] Jing Gu, Yilin Wang, Nanxuan Zhao, Tsu-Jui Fu, Wei Xiong, Qing Liu, Zhifei Zhang, He Zhang, Jianming Zhang, HyunJoon Jung, et al. Photoswap: Personalized subject swapping in images. *Advances in Neural Information Processing Systems*, 36, 2024.
- [12] Eric Hedlin, Gopal Sharma, Shweta Mahajan, Hossam Isack, Abhishek Kar, Andrea Tagliasacchi, and Kwang Moo Yi. Unsupervised semantic correspondence using stable diffusion. *Advances in Neural Information Processing Systems*, 36, 2024.
- [13] Amir Hertz, Ron Mokady, Jay Tenenbaum, Kfir Aberman, Yael Pritch, and Daniel Cohen-Or. Prompt-to-prompt image editing with cross attention control. *arXiv preprint arXiv:2208.01626*, 2022.
- [14] Xun Huang and Serge Belongie. Arbitrary style transfer in real-time with adaptive instance normalization. In *Proceedings of the IEEE international conference on computer vision*, pages 1501–1510, 2017.
- [15] Inbar Huberman-Spiegelglas, Vladimir Kulikov, and Tomer Michaeli. An edit friendly ddpm noise space: Inversion and manipulations. *arXiv preprint arXiv:2304.06140*, 2023.
- [16] Alexander Kirillov, Eric Mintun, Nikhila Ravi, Hanzi Mao, Chloe Rolland, Laura Gustafson, Tete Xiao, Spencer Whitehead, Alexander C Berg, Wan-Yen Lo, et al. Segment anything. In *Proceedings of the IEEE/CVF International Conference on Computer Vision*, pages 4015–4026, 2023.
- [17] Gihyun Kwon and Jong Chul Ye. Diffusion-based image translation using disentangled style and content representation. *arXiv preprint arXiv:2209.15264*, 2022.
- [18] Mingi Kwon, Jaeseok Jeong, and Youngjung Uh. Diffusion models already have a semantic latent space. *arXiv preprint arXiv:2210.10960*, 2022.
- [19] Hyunsoo Lee, Minsoo Kang, and Bohyung Han. Conditional score guidance for text-driven image-to-image translation. *Advances in Neural Information Processing Systems*, 36, 2024.

- [20] Shilin Lu, Yanzhu Liu, and Adams Wai-Kin Kong. Tf-icon: Diffusion-based training-free cross-domain image composition. In *Proceedings of the IEEE/CVF International Conference on Computer Vision*, pages 2294–2305, 2023.
- [21] Grace Luo, Lisa Dunlap, Dong Huk Park, Aleksander Holynski, and Trevor Darrell. Diffusion hyperfeatures: Searching through time and space for semantic correspondence. *Advances in Neural Information Processing Systems*, 36, 2024.
- [22] Chong Mou, Xintao Wang, Jiechong Song, Ying Shan, and Jian Zhang. Dragondiffusion: Enabling drag-style manipulation on diffusion models. *arXiv preprint arXiv:2307.02421*, 2023.
- [23] Chong Mou, Xintao Wang, Jiechong Song, Ying Shan, and Jian Zhang. Diffeditor: Boosting accuracy and flexibility on diffusion-based image editing. *arXiv preprint arXiv:2402.02583*, 2024.
- [24] Taesung Park, Jun-Yan Zhu, Oliver Wang, Jingwan Lu, Eli Shechtman, Alexei Efros, and Richard Zhang. Swapping autoencoder for deep image manipulation. *Advances in Neural Information Processing Systems*, 33:7198–7211, 2020.
- [25] Gaurav Parmar, Krishna Kumar Singh, Richard Zhang, Yijun Li, Jingwan Lu, and Jun-Yan Zhu. Zero-shot image-to-image translation. In *ACM SIGGRAPH 2023 Conference Proceedings*, pages 1–11, 2023.
- [26] Or Patashnik, Daniel Garibi, Idan Azuri, Hadar Averbuch-Elor, and Daniel Cohen-Or. Localizing object-level shape variations with text-to-image diffusion models. In *Proceedings of the IEEE/CVF International Conference on Computer Vision*, pages 23051–23061, 2023.
- [27] Alec Radford, Jong Wook Kim, Chris Hallacy, Aditya Ramesh, Gabriel Goh, Sandhini Agarwal, Girish Sastry, Amanda Askell, Pamela Mishkin, Jack Clark, et al. Learning transferable visual models from natural language supervision. In *International conference on machine learning*, pages 8748–8763. PMLR, 2021.
- [28] Robin Rombach, Andreas Blattmann, Dominik Lorenz, Patrick Esser, and Björn Ommer. High-resolution image synthesis with latent diffusion models. In *Proceedings of the IEEE/CVF conference on computer vision and pattern recognition*, pages 10684–10695, 2022.
- [29] Luming Tang, Menglin Jia, Qianqian Wang, Cheng Perng Phoo, and Bharath Hariharan. Emergent correspondence from image diffusion. *Advances in Neural Information Processing Systems*, 36:1363–1389, 2023.
- [30] Narek Tumanyan, Omer Bar-Tal, Shai Bagon, and Tali Dekel. Splicing vit features for semantic appearance transfer. In *Proceedings of the IEEE/CVF Conference on Computer Vision and Pattern Recognition*, pages 10748–10757, 2022.
- [31] Narek Tumanyan, Michal Geyer, Shai Bagon, and Tali Dekel. Plug-and-play diffusion features for text-driven image-to-image translation. In *Proceedings of the IEEE/CVF Conference on Computer Vision and Pattern Recognition*, pages 1921–1930, 2023.
- [32] Binxin Yang, Shuyang Gu, Bo Zhang, Ting Zhang, Xuejin Chen, Xiaoyan Sun, Dong Chen, and Fang Wen. Paint by example: Exemplar-based image editing with diffusion models. In *Proceedings of the IEEE/CVF Conference on Computer Vision and Pattern Recognition*, pages 18381–18391, 2023.
- [33] Fisher Yu, Ari Seff, Yinda Zhang, Shuran Song, Thomas Funkhouser, and Jianxiong Xiao. Lsun: Construction of a large-scale image dataset using deep learning with humans in the loop. *arXiv preprint arXiv:1506.03365*, 2015.
- [34] Jiwen Yu, Yinhuai Wang, Chen Zhao, Bernard Ghanem, and Jian Zhang. Freedom: Training-free energy-guided conditional diffusion model. In *Proceedings of the IEEE/CVF International Conference on Computer Vision*, pages 23174–23184, 2023.
- [35] Junyi Zhang, Charles Herrmann, Junhwa Hur, Luisa Polania Cabrera, Varun Jampani, Deqing Sun, and Ming-Hsuan Yang. A tale of two features: Stable diffusion complements dino for zero-shot semantic correspondence. *Advances in Neural Information Processing Systems*, 36, 2024.
- [36] Lvmin Zhang, Anyi Rao, and Maneesh Agrawala. Adding conditional control to text-to-image diffusion models. In *Proceedings of the IEEE/CVF International Conference on Computer Vision*, pages 3836–3847, 2023.

Our model has the potential to impact creativity in art domains. However, there are concerns regarding its potential for misuse and copyright issues.

A Implementation details

We apply proposed methods to text-to-image stable diffusion model [28] using checkpoint v1.5. We begin by inverting real images with the edit-friendly DDPM inversion [15], sampling images with 100 denoising timesteps. To find semantic correspondence, we use the feature maps input to the self-attention layer. We set the denoising step $t \in [42, 100]$ and layer $l \in [2, 3]$ from the up-blocks of U-net to find correspondences and rearrange features. Additionally, we apply AdaIN at denoising step $t \in [82, 100]$ and use the off-the-shelf model SAM [16] to obtain object masks. All of the experiments are conducted on an NVIDIA A6000 GPU and during the transfer experiments, the GPU memory usage amounted to about 15.17 GB.

B Evaluation

Quantitative evaluations were conducted in the domains of buildings and animal faces. Building images were obtained from Pexels and Google, comprising 30 pairs of structure images and target images. For the animal face domain, 42 pairs from the AFHQ dataset were used. Ours, Cross-Image [1], DiffEditor [23], and Splice ViT [30] were tested at an image resolution of 512^2 . Swapping AE [24] and DiffuseIT [17] were tested at a resolution of 256^2 .

C Baselines

Cross-Image [1] employs edit-friendly DDPM inversion [15] for image inversion. Images are sampled with 100 denoising timesteps. The KV injection in self-attention occurs at $t \in [42, 100]$ and layer $l \in [2, 3]$ from the up-blocks. The contrast strength is set to 1.65, and the swap guidance scale is set to 3.5. Additionally, for consistency with our model, experiments were conducted using stable diffusion v1.5. Diffeditor is also experimented with under stable diffusion v1.5. We use the standard DDIM scheduler for 50 denoising steps. The classifier-free guidance scale was set to the default value of 5.

DiffuseIT [17] utilizes external models [27, 2] to guide the denoising process. We set the denoising timestep to 200, skipping the initial 80 timesteps, and use a resampling step of $N=10$ (resulting in a total of 130 iterations). Images are resized to a resolution of 224^2 to compute the ViT and CLIP losses, as these models only accept this resolution. These settings is the default configuration for image-guided manipulation as specified by the authors. Additionally, other configurations, including hyperparameters, follow the default settings provided by the authors. Since the provided checkpoint is trained at a resolution of 256^2 , we also conducted experiments at this resolution.

Splice ViT [30] employs a pre-trained DINO ViT model [2] as a feature extractor for optimizing model on a single image pair. We use the 12-layer pre-trained ViT-B/8 model provided in the official DINO ViT implementation. For the ViT loss, images are resized to a resolution of 224^2 . Keys are derived from the deepest attention module for self-similarity, and the output of the deepest layer is used to extract the appearance from the target appearance image. We optimize using an input image pair with a resolution of 512^2 for 2000 iterations. These settings follow the default settings provided by the authors, and other configurations, including hyperparameters, also follow the provided configurations.

D Additional pre vs every matching results

As shown in Figure S1, we present more samples for analysis of semantic matching step. Figure S1 (c) shows unnatural outputs including artifacts, while (d) ours exhibits a more natural appearance compared to the results in (c) and accurately reflects the details of the reference image’s appearance.

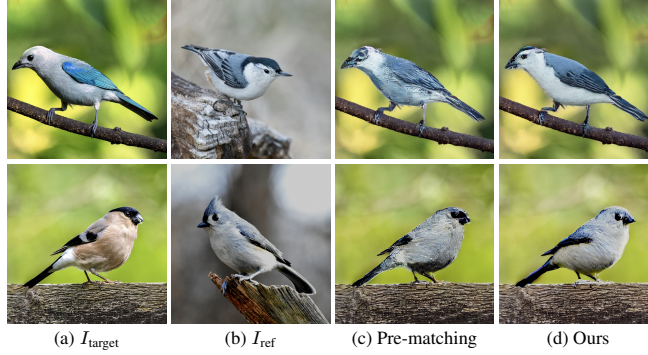


Figure S1: More samples for analysis of semantic matching step

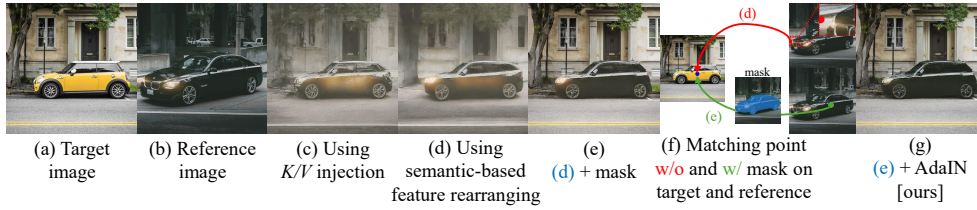


Figure S2: Detail ablation explanation of additional sample

E Additional examples on ablation study

We present additional samples from the ablation study analyzing the effects of each component of our model in Figure S3 and Figure S2.

As shown in Figure S2(e), occasional semantic mismatches, which make the background from contributing in the object region, are prevented by matching within masks. The red arrow indicates incorrect matching to the background. Adding an object mask, as shown by the green arrow, ensures correct semantic matching within the object.

F Additional qualitative results

In Figure S4 and Figure S5, we provide more additional qualitative comparison with Cross-Image [1], Diffeditor [23], DiffuseIT [17], and Splice ViT [30]. Additionally, Figure S6 shows the results of appearance transfer from each object from two different reference images to multiple objects in a single target image. Each appearance transfer process occurs simultaneously.

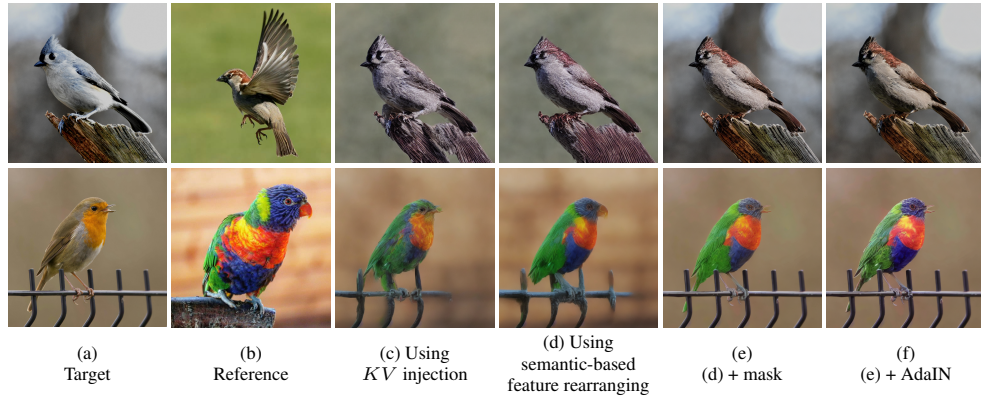


Figure S3: Additional samples of ablation study

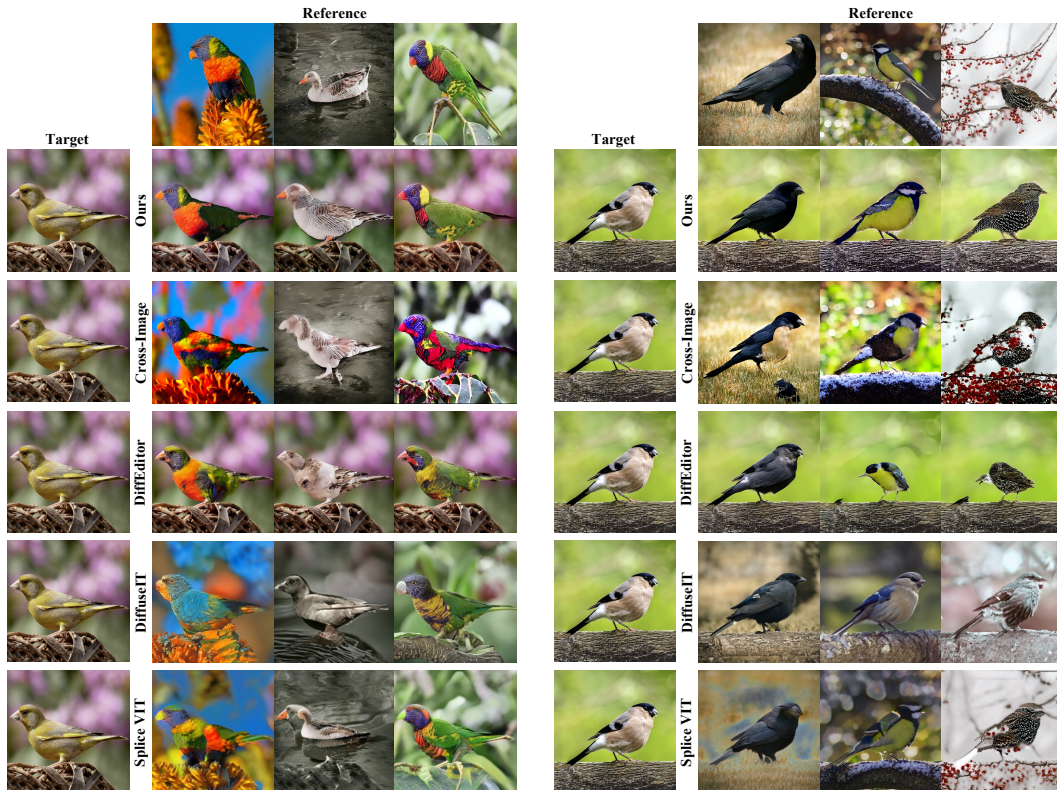


Figure S4: Qualitative comparison of appearance transfer for bird samples with previous works [1, 23, 17, 30]

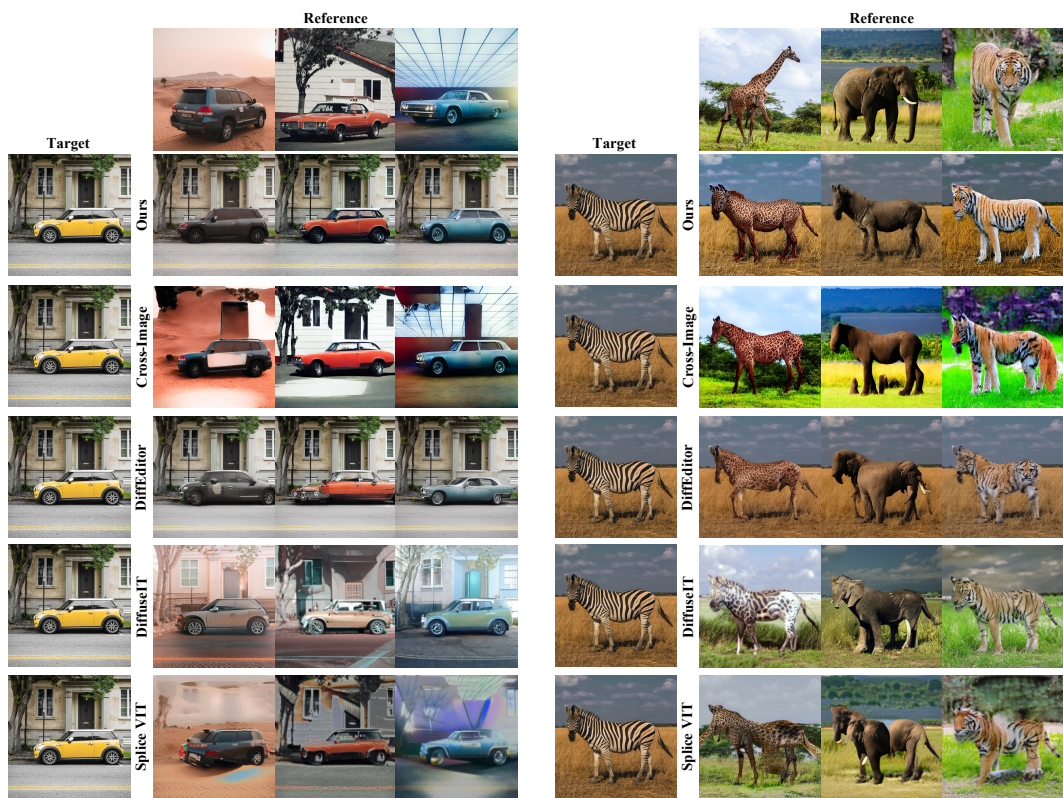


Figure S5: **Qualitative comparison of appearance transfer for car and wild animal samples with previous works [1, 23, 17, 30]**

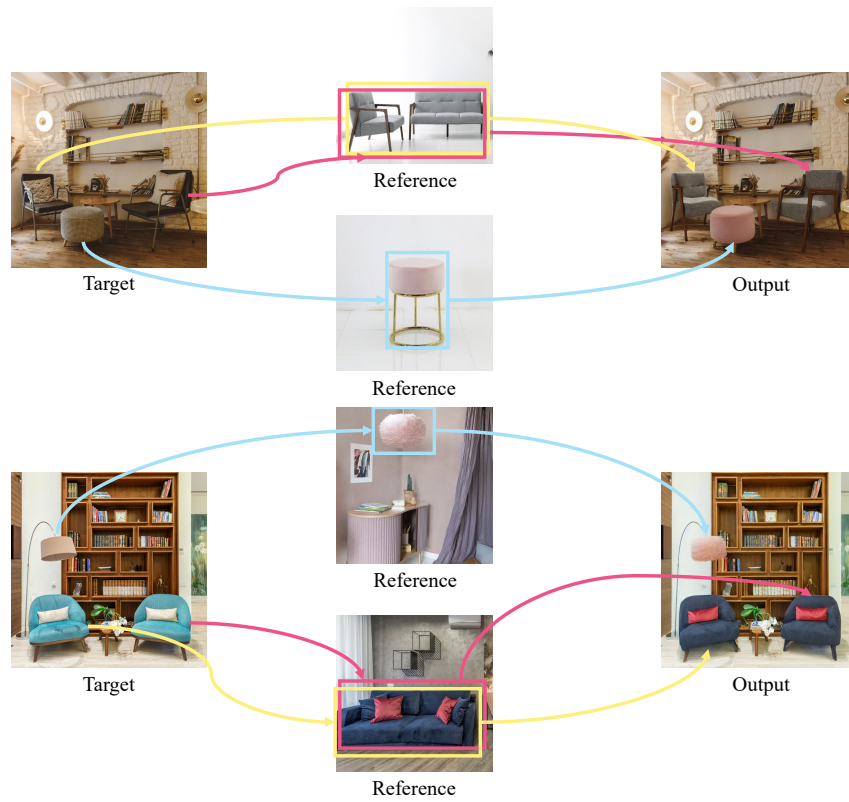


Figure S6: Results of appearance transfer between multiple objects